Research Article

A. Abbasi, W. Farooq, M. Gul, Manish Gupta, Dilsora Abduvalieva, Farwa Asmat*, and Salman A. AlQahtani*

Non-similar modeling and numerical simulations of microploar hybrid nanofluid adjacent to isothermal sphere

https://doi.org/10.1515/phys-2023-0159
received September 03, 2023; accepted November 20, 2023

Abstract: In today's era of rapid technological development, there is an increasing requirement for high-functioning investiture solutions, working liquids and materials that can satisfy the benchmarks of energy efficacy. Specifically, within the domain of heat transference-based industries, an essential challenge is to fabricate a cooling medium that can effectually cope with dissipation of substantial heat flux engendered by high-energy utilizations. At present, nanoliquids are extensively deliberated as some of the most promising aspirants for such effectual cooling mediums. The current investigation features hybrid nanoliquid flow adjacent to magnetized non-isothermal incompressible sphere. Rheological expressions representing micropolar liquid are accounted for flow formulation. The rheological analysis is developed using the boundary-layer concept. Buoyancy impact is accounted for heat transference analysis. Nanoparticles with distinct shapes are considered. The developed nonlinear systems are computed numerically and non-similar simulations are performed.

Keywords: micropolar hybrid nanofluid isothermal sphere, hybrid nanofluids, Keller box method, non-similarity transformations

*** Corresponding author: Farwa Asmat,** School of Mathematical Sciences, Peking University, Beijing 100871, P.R. China, e-mail: farwaasmat@pku.edu.cn
*** Corresponding author: Salman A. AlQahtani,** Computer Engineering Department, College of Computer and Information Sciences, King Saud University, Riyadh, Saudi Arabia, e-mail: salmanq@ksu.edu.sa
A. Abbasi, W. Farooq, M. Gul: Department of Mathematics, University of Azad Jammu and Kashmir, Muzaffarabad 13100, Pakistan
Manish Gupta: Division of Research and Technology, Lovely Professional University, Phagwara, India
Dilsora Abduvalieva: Doctor of Philosophy in Pedagogical Sciences, Tashkent State Pedagogical University, Bunyodkor Avenue, 27, Tashkent, 100070, Uzbekistan

Nomenclature

a	radius of sphere (m)
C_{f}	skin fraction
f	similarity variable
Gr	thermal Grashof number
g_1	gravitational acceleration ($\mathrm{m\,s^{-2}}$)
j	microinertia density
κ	vortex viscosity ($\mathrm{kg\,m^{-1}\,s^{-1}}$)
m	shape factor
$\bar{N}$	micro-rotation vector
Nu	Nussle number
Pr	Prandtl number
$\bar{p}$	pressure
R	micro-rotation parameter
$r(\bar{x})$	distance from axis of symmetry (m)
T_{w}	surface temperature
$\bar{T}$	temperature (K)
T_∞	ambient temperature
$\bar{u}_1, \bar{u}_2$	axial and tangential velocity components ($\mathrm{m\,s^{-1}}$)
u_1, u_2	dimensionless velocity components ($\mathrm{ms^{-1}}$)
$\bar{V}$	velocity field
x, y	dimensionless coordinates (m)
α_{hnf}	thermal diffusivity
ψ	stream function
ρ_{hnf}	density of hybrid nanofluid ($\mathrm{kg\,m^{-3}}$)
θ	dimensionless temperature
γ_{hnf}	gyro-viscosity of hybrid nanofluid
β_{hnf}	thermal expansion coefficient of hybrid nanofluid ($\mathrm{K^{-1}}$)
μ_{hnf}	viscosity of hybrid nanofluid ($\mathrm{kg\,m^{-1}\,s^{-1}}$)
ϕ_1, ϕ_2	solid volume frictions of nanoparticles

1 Introduction

Nanofluids (NFs) are delineated as the fraternization of nanoparticles, characteristically at the nanometer scale

into base liquids, *e.g.*, engine oils, water (W), propylene glycol and ethylene glycol. These nanoparticles possess considerably augmented thermal conductivity in comparison to the aforesaid base liquids. NFs (established by Choi and Eastman [1]) exhibit excellent thermal attributes than base liquids making them favorable for numerous thermal utilizations. The formulation of NFs is feasible by amalgamating with distinct nanoparticles like ZnO_2, graphene oxide, TiO_2, Mn_3O_4, Co_3O_4, ZrO_2, Fe_3O_4, Al_2O_3, Ni, CNTs, SiO_2 and CuO. The magnetized NFs are elaborated through thermal aspects and their ability to maintain flowability in the existence of stronger magnetic field suggest a wide-range diversity of possible utilizations like shock absorbers, gyrating shaft seals, electronic chilling, micro-fluidic pumps, solar collectors, liquid crystal doping, magneto-caloric pumps and bearing lubricants. The biomedical utilizations of magnetized NFs encompass hyperthermia treatment, magnetically guided drug delivery, enhancing contrast in MRI-based scans and seceding cells in bone narrowing samples septic with ailments [2–4]. Researchers accounted various NFs models [5–16] under multi-physical flow conditions and geometries.

Nowadays, liquid flowing problems capturing non-Newtonian rheology have procured substantial importance and efficacy in addressing pragmatic challenges. Liquids featuring non-Newtonian rheology are predominant in numerous industries, encompassing chemicals, oil, petroleum and biofluid mechanics. Such liquids, unlike Newtonian liquids, possess distinguishing aspects, for example, microstructures, disclose behaviors implicating couple stresses, angular momentum, and micro-inertia. For that reason, the classical hydrodynamics relations are inadequate to completely elaborate and comprehend the complications unveiled by non-Newtonian liquids. Liquid crystals, animal blood, muddy fluids, liquids subjected to additives, *etc.*, are such liquids that contain the aforesaid characteristics. Kausar *et al.* [17] first reported micropolar liquid theory based on microstructures. Analysis elaborated by Kausar *et al.* [17] is accounted by various researchers subjected to diverse mathematical assumptions. Patel *et al.* [18] mathematical study of unsteady micropolar fluid flow due to nonlinear stretched sheet in the presence of magnetic field. Time-dependent stretching flow featuring magnetized micropolar liquid under porosity, Robin conditions, Ohmic dissipation and chemical reaction is formulated by Thenmozhi *et al.* [19]. Yadav *et al.* [20] scrutinized entropy generation analysis in micropolar couple stress fluid's flow in an inclined porous channel using Homotopy Analysis Method. Magyar *et al.* [21] combined effect of heat generation or absorption and first-order chemical reaction on micropolar fluid flows over a uniformly stretched permeable surface. Mustafa *et al.* [22] find non-similar solution for a power-law fluid flow over a moving wedge.

Lie group analysis is the method which is used to find the similarity variables that transform the partial differential equations for engineering boundary value problems to ordinary differential equations. This method based on the invariant conditions but these conditions do not possess by some partial differential equations such as the governing equations for the flow of non-Newtonian fluid past a Wedge at an oblique angle [23], viscous dissipative flow [24] *etc.,* in these situations non-local similar or non-similar solutions of the governing equations over can be obtained. Chamkha *et al.* [25] applied local non-similarity method to develop the equations for convective flow over c cylinder. Kong and Liu [26], Lyu *et al.* [27] and Qiu *et al.* [28] explored the applications of micro-spectroscopy under pressure, characteristics of cavity dynamics and spatial confinement in fiber-optic laser respectively. Qiu *et al.* [29] and Zhao *et al.* [30] worked on chlorine emission characteristics on cement pastes and sub-microscale uncertainty measurement method using pattern recognition. Non-similar solutions method have been used in recent years to discuss flows, coupled heat and mass transfer in different geometries under the various physical conditions [31–36]. Previous literature [41–46] highlight some recent development in fluid flow *via* various flow assumptions.

Thermal analysis of hybrid NFs due to their applications in paint industry, electronic chips and mechanical engineering is an interesting topic and the only similar solution to the governing equations for the flow of these fluids are available in literature. Modeling and non-similar solution for the governing equations for the flows of hybrid NFs are interesting and challenging issues from a mathematical point of view. The present exploration accounts for dual convection importance in hybrid nanoliquid flow adjacent to magnetized non-isothermal incompressible sphere. Micropolar liquid is considered to formulate the boundary layer convective flow. The developed nonlinear systems are computed numerically and non-similar simulations are performed. The outcomes are graphically illustrated and subsequently analyzed for interpretation.

2 Formulation of the problem

Consider the free convective transport of water-based micropolar hybrid NF adjacent to non-isothermal sphere. The magnetized flow of incompressible micropolar hybrid NF over a sphere having radius a and heated to temperature T_w is considered as presented in Figure 1. The temperature at free stream is considered to be T_∞. The x coordinate is taken along the external of the sphere and y coordinate is taken normal to the surface of sphere.

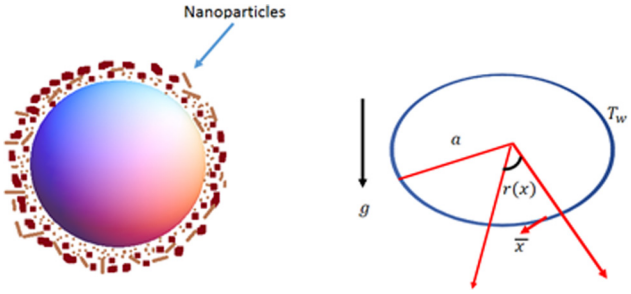

Figure 1: Geometry of the problem.

Furthermore, the radiated space (r) is chosen from symmetric axes to $r = \text{asin}\,(x/a)$ surface. The gravity acts in downwards direction of the sphere. The flow region is under the impact of strong transverse magnetic field $\vec{B} = (0, B_0, 0)$. By employing the conservation laws on boundary conditions, the following boundary layer equations for the problem are follows as

The fundamental conservation laws under present assumptions are [32,37] as follows:

$$\nabla.\ \bar{\boldsymbol{V}} = 0,\ \text{(continuity equation)}, \tag{1}$$

$$\rho_{\text{hnf}}\frac{\text{D}\bar{\boldsymbol{V}}}{\text{D}\bar{t}} = -\bar{\nabla}\bar{p} + (\mu_{\text{hnf}} + \kappa)\bar{\nabla}^2\bar{\boldsymbol{V}} + \kappa(\bar{\nabla}\times\bar{\boldsymbol{N}}) + \bar{\boldsymbol{F}},\ \text{(linear momentum equation)}, \tag{2}$$

$$\rho_{\text{hnf}}\, j\frac{\text{D}\bar{\boldsymbol{N}}}{\text{D}\bar{t}} = \gamma_{\text{hnf}}\bar{\nabla}^2\bar{\boldsymbol{N}} + \kappa(\bar{\nabla}\times\bar{\boldsymbol{V}} - 2\bar{\boldsymbol{N}}),\ \text{(micro rotation equation)}, \tag{3}$$

$$\frac{\text{D}\bar{T}}{\text{D}\bar{t}} = \alpha_{\text{hnf}}\nabla^2\bar{T},\ \text{(energy equation)}, \tag{4}$$

where $\boldsymbol{V} = (\bar{u}_1, \bar{u}_2, 0)$ is the velocity of hybrid NF, $\bar{T}$ is the temperature of hybrid NF, $\bar{p}$ is the pressure, $\bar{\boldsymbol{N}}$ is the micro-rotation vector and κ is the vortex viscosity. Furthermore, ρ_{hnf} is the density of hybrid NF, μ_{hnf} is the viscosity of hybrid NF and α_{hnf} is the thermal diffusivity of hybrid NF. Also, j stands for microinertia per unit mass and $\bar{\boldsymbol{F}} = \bar{\boldsymbol{J}} \times \bar{\boldsymbol{B}}$ and $g_1(\rho\beta)_{\text{hnf}}(\bar{T} - T_\infty)\sin\left(\frac{\bar{x}}{a}\right)$, where g stands for gravitational acceleration and β_{hnf} stands for the thermal expansion coefficient of hybrid NF. By using basic equation of magneto hydrodynamics $\bar{\boldsymbol{J}} \times \bar{\boldsymbol{B}} = -(-\sigma_{\text{hnf}}B_0^2\bar{u}_1, \sigma_{\text{hnf}}B_0^2\bar{u}_2, 0)$, in which σ_{hnf} is the electric conductivity of hybrid NF.

Under the Boussinesq boundary layer approximations, the governing equations are as follows [32]:

$$\frac{\partial(r\bar{u}_1)}{\partial\bar{x}} + \frac{\partial(r\bar{u}_2)}{\partial\bar{y}} = 0, \tag{5}$$

$$\rho_{\text{hnf}}\left(\bar{u}_1\frac{\partial\bar{u}_1}{\partial\bar{x}} + \bar{u}_2\frac{\partial\bar{u}_1}{\partial\bar{y}}\right) = (\mu_{\text{hnf}} + \kappa)\frac{\partial^2\bar{u}_1}{\partial\bar{y}^2} + \kappa\frac{\partial\bar{N}}{\partial\bar{y}} - \sigma_{\text{hnf}}B_0^2\bar{u}_1 + g_1(\rho\beta)_{\text{hnf}}(\bar{T} - T_\infty)\sin\left(\frac{\bar{x}}{a}\right), \tag{6}$$

$$\rho_{\text{hnf}}\, j\left(\bar{u}_1\frac{\partial\bar{N}}{\partial\bar{x}} + \bar{u}_2\frac{\partial\bar{N}}{\partial\bar{y}}\right) = \gamma_{\text{hnf}}\frac{\partial^2\bar{N}}{\partial\bar{y}^2} - \kappa\left(\frac{\partial\bar{u}_1}{\partial\bar{y}} + 2\bar{N}\right), \tag{7}$$

$$\bar{u}_1\frac{\partial\bar{T}}{\partial\bar{x}} + \bar{u}_2\frac{\partial\bar{T}}{\partial\bar{y}} = \alpha_{\text{hnf}}\frac{\partial^2\bar{T}}{\partial\bar{y}^2}, \tag{8}$$

where $\bar{u}_1$ is the velocity component along $\bar{x}$-axis and $\bar{u}_2$ is the velocity component along $\bar{y}$-axis and $\gamma_{\text{hnf}} = \left(\mu_{\text{hnf}} + \frac{\kappa}{2}\right)j$ stands for the vortex viscosity of hybrid NF. The appropriate conditions for the flow and heat transfer for the flow over fixed solid sphere are given in Table 1.

$$\bar{u}_1 = \bar{u}_2 = 0, \bar{N} = \frac{1}{2}\frac{\partial\bar{u}_1}{\partial\bar{y}}, \bar{T} = T_w \quad \text{on} \quad \bar{y} = 0, \tag{9}$$

$$\bar{u}_1 = 0, \bar{T} = T_\infty \quad \text{on} \quad \bar{y} \to \infty. \tag{10}$$

In which, ϕ_1 represents the solid volume fraction of Fe_3O_4 nanoparticles and ϕ_2 denotes the solid volume fraction of $CoFe_2O_4$ nanoparticles. The subscript f stands for the properties of base fluid which is water (H_2O) and s_1 denotes the properties of Fe_3O_4 and s_2 of $CoFe_2O_4$. Also, m is

Table 1: Thermo-physical properties of hybrid NF [37,38]

Viscosity	$\mu_{\text{hnf}} = \frac{\mu_{\text{f}}}{(1-\phi_1)^{2.5}(1-\phi_2)^{2.5}}$
Density	$\rho_{\text{hnf}} = (1-\phi_1)(1-\phi_2)\rho_{\text{f}} + \phi_1\rho_{s_1} + \phi_2\rho_{s_2}$
Heat capacity	$(\rho C_{\text{p}})_{\text{hnf}} = (1-\phi_1)(1-\phi_2)(\rho C_{\text{p}})_{\text{f}} + \phi_1(\rho C_{\text{p}})_{s_1} + \phi_2(\rho C_{\text{p}})_{s_2}$
Specific heat	$(\rho\beta)_{\text{hnf}} = (1-\phi_1)(1-\phi_2)(\rho\beta)_{\text{f}} + \phi_1(\rho\beta)_{s_1} + \phi_2(\rho\beta)_{s_2}$
Thermal conductivity	$\frac{K_{\text{hnf}}}{K_{\text{bf}}} = \frac{K_{s_2} + (m-1)K_{\text{bf}} - (m-1)\phi_2(K_{\text{bf}} - K_{s_2})}{K_{s_2} + (m-1)K_{\text{bf}} + \phi_2(K_{\text{bf}} - K_{s_2})}$, where $\frac{K_{\text{bf}}}{K_{\text{f}}} = \frac{K_{s_1} + (m-1)K_{\text{f}} - (m-1)\phi_1(K_{\text{f}} - K_{s_1})}{K_{s_1} + (m-1)K_{\text{f}} + \phi_1(K_{\text{f}} - K_{s_1})}$
Electric conductivity	$\frac{\sigma_{\text{hnf}}}{\sigma_{\text{bf}}} = \frac{\sigma_{s_1} + 2\sigma_{\text{bf}} - 2\phi_2(\sigma_{\text{bf}} - \sigma_{s_1})}{\sigma_{s_1} + 2\sigma_{\text{bf}} + \phi_2(\sigma_{\text{bf}} - \sigma_{s_1})}$, where $\sigma_{\text{bf}} = \frac{\sigma_{s_2} + 2\sigma_{\text{f}} - 2\phi_1(\sigma_{\text{f}} - \sigma_{s_2})}{\sigma_{s_2} + 2\sigma_{\text{f}} + \phi_1(\sigma_{\text{f}} - \sigma_{s_2})}\sigma_{\text{f}}$

Table 2: Numerical values of shape factor for different shapes of nanoparticles [39]

Different shapes of nanoparticles	Numerical values
Bricks	3.7
Cylinders	4.9
Platelets	5.7
Blades	8.6

the shape factor, the numerical values of different shapes of nanoparticles is presented in Tables 2 and 3.

The flow and heat transfer Eqs. (5)–(8) with its boundary conditions (9) and (10) by employing the dimensionless variables are given below as:

$$x = \frac{\bar{x}}{a}, y = \mathrm{Gr}^{\frac{1}{4}}\frac{\bar{y}}{a}, u_1 = \left(\frac{a}{\nu_{\mathrm{bf}}}\right)\mathrm{Gr}^{-\frac{1}{2}}\bar{u}_1,$$
$$u_2 = \left(\frac{a}{\nu_{\mathrm{bf}}}\right)\mathrm{Gr}^{-\frac{1}{4}}\bar{u}_2, \theta = \frac{\bar{T} - T_{\mathrm{w}}}{T_{\mathrm{w}} - T_{\infty}}, N = \left(\frac{a^2}{\nu_{\mathrm{bf}}}\right)\mathrm{Gr}^{-\frac{3}{4}}\bar{N}, \tag{11}$$

where Gr represent the thermal Grashof number and u_1, u_2, θ, N, y represent the dimensionless coordinates, velocities, temperature and micro-rotation respectively. The microinertia density is $j = a^2\mathrm{Gr}^{-1/2}$. After using the above variables, the governing equations takes the form

$$\frac{\partial(ru_1)}{\partial x} + \frac{\partial(ru_2)}{\partial y} = 0, \tag{12}$$

$$u_1\frac{\partial u_1}{\partial x} + u_2\frac{\partial u_1}{\partial y} = \frac{\rho_{\mathrm{bf}}}{\rho_{\mathrm{hnf}}}\left(\frac{\mu_{\mathrm{hnf}}}{\mu_{\mathrm{bf}}} + R\right)\frac{\partial^2 u_1}{\partial y^2} + R\frac{\rho_{\mathrm{bf}}}{\rho_{\mathrm{hnf}}}\frac{\partial N}{\partial y} + \frac{(\rho\beta)_{\mathrm{hnf}}}{(\rho\beta)_{\mathrm{bf}}}\frac{\rho_{\mathrm{bf}}}{\rho_{\mathrm{hnf}}}\theta\sin x - \frac{\rho_{\mathrm{bf}}}{\rho_{\mathrm{hnf}}}\frac{\sigma_{\mathrm{hnf}}}{\sigma_{\mathrm{bf}}}\mathrm{Ha}^2 u_1, \tag{13}$$

$$u_1\frac{\partial N}{\partial x} + u_2\frac{\partial N}{\partial y} = \frac{\rho_{\mathrm{bf}}}{\rho_{\mathrm{hnf}}}\left(\frac{\mu_{\mathrm{hnf}}}{\mu_{\mathrm{bf}}} + \frac{R}{2}\right)\frac{\partial^2 N}{\partial y^2} - R\frac{\rho_{\mathrm{bf}}}{\rho_{\mathrm{hnf}}}\left(\frac{\partial u_1}{\partial y} + 2N\right), \tag{14}$$

$$u_1\frac{\partial\theta}{\partial\bar{x}} + u_2\frac{\partial\theta}{\partial y} = \frac{\alpha_{\mathrm{hnf}}}{\alpha_{\mathrm{bf}}}\frac{1}{\mathrm{Pr}}\frac{\partial^2\theta}{\partial y^2}, \tag{15}$$

where $\left(R = \frac{\kappa}{\mu_{\mathrm{bf}}}, \mathrm{Ha} = \frac{\sigma_{\mathrm{f}}B_0^2a^2}{\rho_{\mathrm{f}}(\mathrm{Gr})^{1/2}}, \mathrm{Pr} = \frac{\nu_{\mathrm{bf}}}{\alpha_{\mathrm{bf}}}\right)$ are dimensionless micro-rotation parameter, Hartman number and Prandtl number. The dimensionless boundary conditions can be expressed as follows:

$$u_1 = u_2 = 0, N = \frac{1}{2}\frac{\partial u_1}{\partial y}, \theta = 1 \quad \text{on} \quad y = 0, \tag{16}$$

$$u_1 = 0, \theta = 0 \quad \text{on} \quad y \to \infty, \tag{17}$$

The stream function $\psi = xr(x)f(x,y)$ is related to velocity components such that $u_1 = (1/r)\partial\psi/\partial y$ and $u_2 = -(1/r)\partial\psi/\partial x$ and dependent variables $\theta = \theta(x,y)$ and $N = xg(x,y)$ to reduce the number of dependent variables in the governing equations; the governing equations are as follows:

$$\frac{(A_2 + R)}{A_1}f''' + \left(1 + \frac{x}{\sin x}\cos x\right)ff'' + \frac{R}{A_1}g' - (f')^2 + \frac{A_3}{A_1}\theta\frac{\sin x}{x} - \frac{A_4}{A_1}\mathrm{Ha}^2f' = x\left(f'\frac{\partial f'}{\partial x} - f''\frac{\partial f}{\partial x}\right), \tag{18}$$

$$\frac{\left(A_2 + \frac{R}{2}\right)}{A_1}g'' + \left(1 + \frac{x}{\sin x}\cos x\right)fg' - gf' - \frac{R}{A_1}(2g + f'') = x\left(f'\frac{\partial g}{\partial x} - \frac{\partial f}{\partial x}g'\right), \tag{19}$$

$$\frac{1}{\mathrm{Pr}}\frac{\alpha_{\mathrm{hnf}}}{\alpha_{\mathrm{bf}}}\theta'' + \left(1 + \frac{x}{\sin x}\cos x\right)f\theta' = x\left(f'\frac{\partial\theta}{\partial x} - \frac{\partial f}{\partial x}\theta'\right), \tag{20}$$

where $A_1 = \frac{\rho_{\mathrm{hnf}}}{\rho_{\mathrm{f}}}$, $A_2 = \frac{\mu_{\mathrm{hnf}}}{\mu_{\mathrm{bf}}}$, $A_3 = \frac{(\rho\beta)_{\mathrm{hnf}}}{(\rho\beta)_{\mathrm{bf}}}$, $A_4 = \frac{\sigma_{\mathrm{hnf}}}{\sigma_{\mathrm{bf}}}$ and $A_5 = \frac{\alpha_{\mathrm{hnf}}}{\alpha_{\mathrm{bf}}}$.

After using the stream function and dependent variables, the relevant boundary conditions takes the form

$$f = 0 = f', \theta = 1 \quad \text{at} \quad y = 0,$$
$$f' = 0, \theta = 0 \quad \text{at} \quad y \to \infty. \tag{21}$$

The dimensionless mathematical expression for skin friction and Nusselt number are as follows:

Table 3: Properties of nanoparticles and the base fluid [40]

Properties	Density (ρ)	Specific heat (C_{p})	Thermal conductivity (K)	Thermal expansion coefficient $\beta \times 10^{-5}$	Electric conductivity (σ)
H_2O	997.0	4,179	0.6071	210	5.5×10^{-7}
Fe_3O_4	5,180	670	9.7	1.3	0.74×10^{6}
$CoFe_2O_4$	4,907	700	3.7	1.3	1.1×10^{7}

$$\frac{1}{2}\frac{C_f}{\mathrm{Gr}^{3/4}} = \left(A_2 + \frac{R}{2}\right)x(f'')_{y=0}, \tag{22}$$

$$\frac{\mathrm{Nu}}{\sqrt[4]{\mathrm{Gr}}} = -\frac{K_{\mathrm{hnf}}}{K_{\mathrm{bf}}}(\theta')_{y=0}. \tag{23}$$

3 Solution methodology

Many numerical methods are proposed and implemented by mathematicians and scientists for boundary layer flows. Keller box method has advantages over these methods due to second order accuracy and easy in programming. The governing Eqs. (18)–(20) subject to boundary conditions (21) are simulated for involved dependent variables by using Keller box method. The numerical scheme is applied in four steps.

Step 1: First, we reduce the governing equations into a system of first order equation by considering

$f' = U, P' = V, g' = W, \theta = S, \theta' = t$, we have

$$\begin{aligned}&\frac{(A_2+R)}{A_1}V' + \left(1 + \frac{x}{\sin x}\cos x\right)fV + \frac{R}{A_1}W \\ &- (U)^2 + \frac{A_3}{A_1}S\frac{\sin x}{x} - \frac{A_4}{A_1}\mathrm{Ha}^2U = x\left(U\frac{\partial U}{\partial x} - V\frac{\partial f}{\partial x}\right),\end{aligned} \tag{24}$$

$$\begin{aligned}&\frac{\left(A_2+\frac{R}{2}\right)}{A_1}W' + \left(1 + \frac{x}{\sin x}\cos x\right)fW - gU - \frac{R}{A_1}(2g+V) \\ &= x\left(U\frac{\partial g}{\partial x} - \frac{\partial f}{\partial x}W\right),\end{aligned} \tag{25}$$

$$\frac{1}{\mathrm{Pr}}\frac{\alpha_{\mathrm{hnf}}}{\alpha_{\mathrm{bf}}}S' + \left(1 + \frac{x}{\sin x}\cos x\right)fS = x\left(U\frac{\partial\theta}{\partial x} - \frac{\partial f}{\partial x}S\right), \tag{26}$$

in which prime is derivative of dependent variables with respect to y, The boundary conditions take the form

$$\begin{aligned}f = 0 = U, S = 1 \quad \text{at} \quad y = 0,\\ U = 0, S = 0 \quad \text{at} \quad y \to \infty.\end{aligned} \tag{27}$$

Step 2: The derivatives of dependent quantities are approximated by central difference and rest of dependent variables by taking mean values, the system of governing equation can be written as follows:

$$f_j^n - f_{j-1}^n = \frac{\Delta y}{2}(U_j^n + U_{j-1}^n), \tag{28}$$

$$U_j^n - U_{j-1}^n = \frac{\Delta y}{2}(V_j^n + V_{j-1}^n), \tag{29}$$

$$g_j^n - g_{j-1}^n = \frac{\Delta y}{2}(W_j^n + W_{j-1}^n), \tag{30}$$

$$S_j^n - S_{j-1}^n = \frac{\Delta y}{2}(t_j^n + t_{j-1}^n), \tag{31}$$

$$\begin{aligned}&\frac{(A_2+R)}{A_1}\frac{V_j^n - V_{j-1}^n}{\Delta y} + \left(1 + \frac{x}{\sin x}\cos x\right)f^n_{j-\frac{1}{2}}V^n_{j-\frac{1}{2}} \\ &+ \frac{R}{A_1}W_{j-\frac{1}{2}^n} - U^n_{j-\frac{1}{2}^2} - \frac{x}{\Delta x}U^n_{j-\frac{1}{2}^2} \\ &+ \frac{x}{\Delta x}\left(f^n_{j-\frac{1}{2}}V^n_{j-\frac{1}{2}} + f^n_{j-\frac{1}{2}}V^{n-1}_{j-\frac{1}{2}}\right) + \frac{A_3}{A_1}S^n_{j-\frac{1}{2}}\frac{\sin x}{x} \\ &- \frac{A_4}{A_1}\mathrm{Ha}^2U^n_{j-\frac{1}{2}} = [R_1]_{j-\frac{1}{2}^{n-1}},\end{aligned} \tag{32}$$

$$\begin{aligned}&\frac{\left(A_2+\frac{R}{2}\right)}{A_1}\frac{W_j^n - W_{j-1}^n}{\Delta y} + \left(1 + \frac{x}{\sin x}\cos x\right)f^n_{j-\frac{1}{2}}W^n_{j-\frac{1}{2}} \\ &- \frac{R}{A_1}\left(2g^n_{j-\frac{1}{2}} + V^n_{j-\frac{1}{2}}\right) - g^n_{j-\frac{1}{2}}U^n_{j-\frac{1}{2}} \\ &- \frac{x}{\Delta x}\left(g^n_{j-\frac{1}{2}}U^{n-1}_{j-\frac{1}{2}}\right) - \frac{x}{\Delta x}\left(g^{n-1}_{j-\frac{1}{2}}U^n_{j-\frac{1}{2}}\right) = [R_3]_{j-\frac{1}{2}^{n-1}},\end{aligned} \tag{33}$$

$$\begin{aligned}&\frac{1}{\mathrm{Pr}}A_5\frac{t_j^n - t_{j-1}^n}{\Delta y} + \left(1 + \frac{x}{\Delta x} + \frac{x}{\sin x}\cos x\right)(ft)^n_{j-\frac{1}{2}} \\ &- \frac{x}{\Delta x}\left(U^n_{j-\frac{1}{2}}S^n_{j-\frac{1}{2}}\right) \\ &+ \frac{x}{\Delta x}\left(U^n_{j-\frac{1}{2}}S^{n-1}_{j-\frac{1}{2}}\right) + \frac{x}{\Delta x}\left(f^n_{j-\frac{1}{2}}t^{n-1}_{j-\frac{1}{2}}\right) = [R_2]_{j-\frac{1}{2}^{n-1}}.\end{aligned} \tag{34}$$

Step 3: In this step, obtained system of non-linear Eqs. (32)–(34) is linearized by using following iterations for unknowns:

$$\begin{aligned}&\delta f_j^n = f_j^n + \delta f_j^n, \delta U_j^n = U_j^n + \delta U_j^n, \delta V_j^n = V_j^n + \delta V_j^n,\\ &\delta g_j^n = g_j^n + \delta g_j^n, \delta W_j^n = W_j^n + \delta W_j^n, \delta S_j^n = S_j^n + \delta S_j^n.\end{aligned} \tag{35}$$

After ignoring $O(\delta^2)$ terms, the resulting linearized algebraic equations are as follows:

$$\delta f_j - \delta f_{j-1} - \frac{\Delta y}{2}(\delta U_j + \delta U_{j-1}) = (r_1)_{j-\frac{1}{2}}, \tag{36}$$

$$\delta U_j - \delta U_{j-1} - \frac{\Delta y}{2}(\delta V_j + \delta V_{j-1}) = (r_2)_{j-\frac{1}{2}}, \tag{37}$$

$$\delta g_j - \delta g_{j-1} - \frac{\Delta y}{2}(\delta W_j + \delta W_{j-1}) = (r_3)_{j-\frac{1}{2}}, \tag{38}$$

$$\delta S_j - \delta S_{j-1} - \frac{\Delta y}{2}(\delta t_j + \delta t_{j-1}) = (r_4)_{j-\frac{1}{2}}, \tag{39}$$

$$\begin{aligned}&a_1\delta V_j + a_2\delta V_{j-1} + a_3\delta f_j + a_4\delta f_{j-1} + a_5\delta U_j + a_6\delta U_{j-1} \\ &+ a_7\delta\theta_j + a_8\delta\theta_{j-1} + a_9\delta P_j + \xi_{a_{10}}\delta P_{j-1} = (r_5)_{j-\frac{1}{2}},\end{aligned} \tag{40}$$

$$b_1\delta t_j + b_2\delta t_{j-1} + b_3\delta S_j + b_4\delta S_{j-1} + b_5\delta f_j + b_6\delta f_{j-1} + b_7\delta U_j + b_8\delta U_{j-1} = (r_6)_{j-\frac{1}{2}}, \quad (41)$$

$$c_1\delta W_j + c_2\delta W_{j-1} + c_3\delta f_j + c_4\delta f_{j-1} + c_5\delta U_j + c_6\delta U_{j-1} + c_7\delta g_j + c_8\delta g_{j-1} + c_9\delta V_j + c_{10}\delta V_{j-1} = (r_7)_{j-\frac{1}{2}}, \quad (42)$$

Step 4: The Eqs. (36)–(42) are decomposed by block elimination method having block tridiagonal structure. Usually, the tridiagonal structure of block matrices having the order of 7 × 7 are computed for the unknowns with forward and backward sweeps. The whole process is implemented in computational software MATLAB.

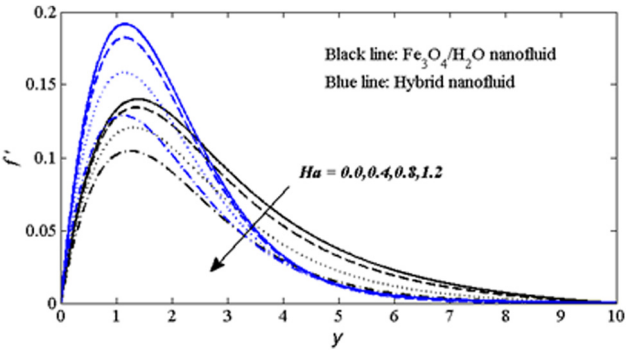

Figure 3: Impact of M on axial velocity f' with $R = x = 0.1$, Pr = 6.2 and $m = 8.6$.

4 Results and discussion

This section presents the impact of micro-rotation parameter R and the magnetic parameter Ha on the different flow features for both traditional NF Fe_3O_4/H_2O based NF and hybrid NF. Figure 2 demonstrates the impact of micro-rotation parameter R on the axial velocity for both types of NFs under consideration. For traditional Fe_3O_4/H_2O NF, the solid volume fraction of Fe_3O_4 nanoparticles is considered to be about 10% while in case of hybrid NF, the solid volume of fraction of both types of nanoparticles Fe_3O_4 and $CoFe_2O_4$ is considered to be 10 and 20% approximately. The response of axial velocity f' near the surface of the sphere and in the free stream region is opposite for enlarging the micro-rotation of microstructure in the traditional NF and hybrid NF. The axial velocity rises near the surface of the sphere with the increase in the micro-rotation factor, while it decreases in the free stream region. The velocity has small magnitude for traditional NF while the boost in the velocity is noticed for the case of hybrid NF. It is an important fact that micro-rotation plays a key role in controlling the movement of the fluid near the surface and this feature is negligible in the free stream region. Figure 3 is plotted to analyze the response of magnetic parameter Ha on the axial velocity f' for both types of NFs. The velocity profile shows a decreasing trend for the increasing values of magnetic parameter for both types of NFs. It is noted that the magnetic force acts as a resistive force on the transport of both types of ferromagnetic nanoparticles adjacent to the surface of the sphere. The effects of magnetic parameter are dismissed in the free stream region. Furthermore, the velocity of the hybrid NF is squeezed in the free stream region and due to both types of ferromagnetic nanoparticles, this response is dominant. Figure 4 demonstrates the impact of axial-coordinate on the axial velocity of traditional Fe_3O_4/H_2O NF and hybrid NF over the surface of solid sphere. It is also observed that the axial velocity of hybrid NF and traditional NF reduces near the surface of the sphere while rises in the rest region.

The rotational velocity of hybrid NF and traditional Fe_3O_4/H_2O NF is reported in Figure 5 for various values of micro-rotation parameter. It is noted that the rise in micro-rotation parameter rises the rotational velocity of both types of NFs. The rotational velocity is minimum in magnitude in the absence of microstructure in the

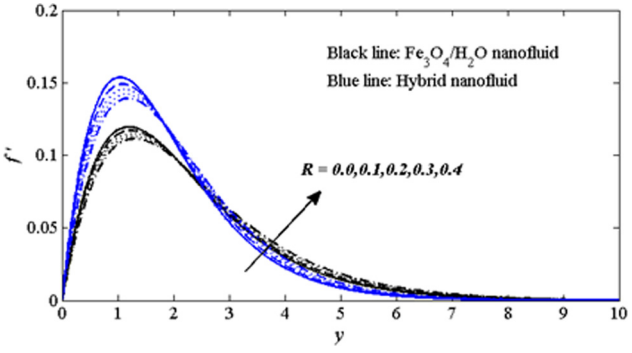

Figure 2: Impact of R on axial velocity f' with $M = 1.0$, $x = 0.1$, Pr = 6.2 and $m = 8.6$.

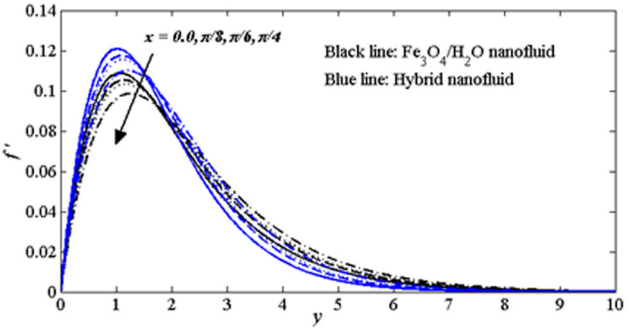

Figure 4: Impact of x on axial velocity f' with $R = M = 1.0$, Pr = 6.2 and $m = 8.6$.

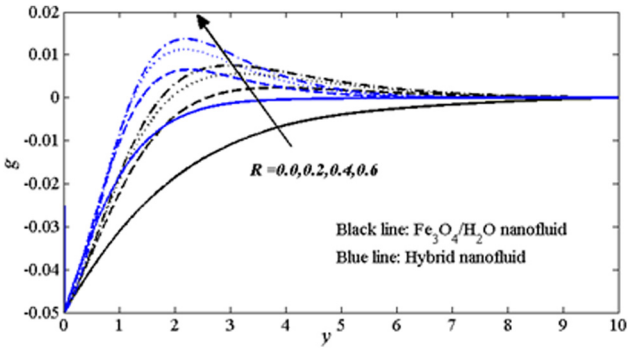

Figure 5: Impact of R on rotational velocity g with M = 1.0, x = 0.1, Pr = 6.2 and m = 8.6.

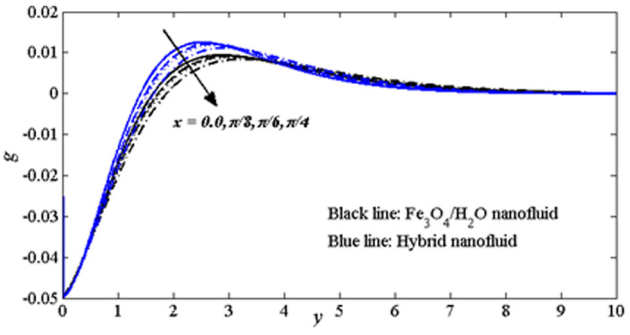

Figure 7: Impact of x on rotational velocity g with R = M = 1.0, Pr = 6.2 and m = 8.6.

traditional NF as well as hybrid NF. The impact of magnetic parameter M on the rotational velocity is reported in Figure 6 for both the types of NFs. The rotational velocity increases near the surface of the sphere at small scale and after this, the increase in the rotational velocity is noticed. Figure 7 demonstrates the impact of x-coordinate on the rotational velocity. The analysis is presented for both traditional NF and hybrid NF and it is noted that near the surface of the sphere, the velocity declines as axial-coordinate moves towards π. The temperature profile is an increasing function of micro-rotation parameter R for Fe_3O_4/H_2O based NF as well as hybrid NF as shown in Figure 8. The micro-rotation plays a key role in the rise in the temperature of NFs. Actually, due to the rise in the microstructure rotation in NFs, the thermal characteristics of the NFs also rises which rises the internal kinetic energy of the base fluid. As a result, the rise in the temperature of the hybrid NF at large scale is noticed with the micro-rotation of microstructure. In Figure 9, the effects of magnetic parameter Ha on the temperature profile are illustrated for both types of NFs under consideration. It is observed that the rise in the magnetic force cause remarkable

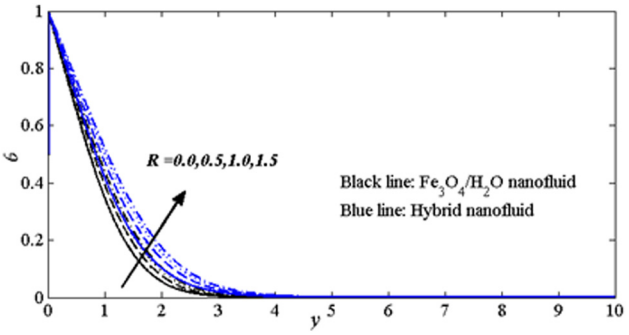

Figure 8: Impact of R on temperature θ with M = 1.0, x = 0.1, Pr = 6.2 and m = 8.6.

resistance to the flow and as a result, the collusion between the nanoparticles in the liquid rises. Due to this reason, the internal kinetic energy of NFs rises which boosts the temperature of NFs. In Figure 10, the temperature profile is plotted against x-coordinate for traditional NF and hybrid NF over an isothermal surface of the sphere. It is noticed that as we move from 0 to π, the temperature of both types of NF rises over the surface of sphere. Figure 11 is plotted to explore the impact of different shapes of nanoparticles on

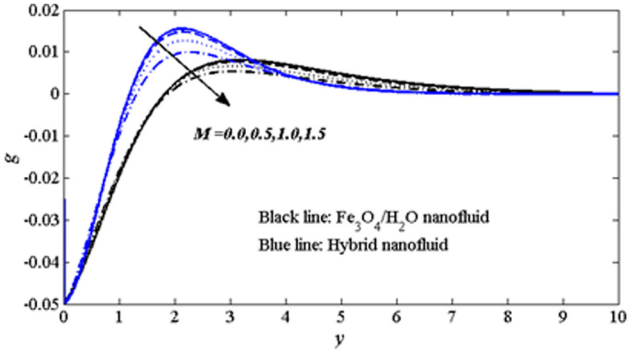

Figure 6: Impact of M on rotational velocity g with R = x = 0.1, Pr = 6.2 and m = 8.6.

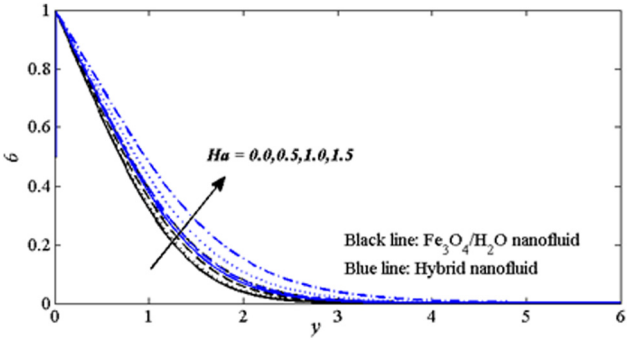

Figure 9: Impact of M on temperature θ with R = x = 0.1, Pr = 6.2 and m = 8.6.

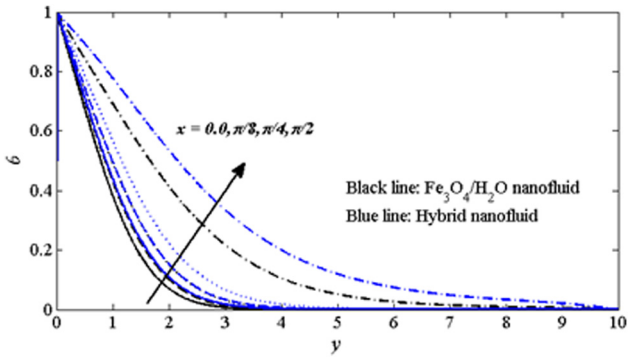

Figure 10: Impact of x on temperature θ with $R = M = 1.0$, Pr = 6.2 and $m = 8.6$.

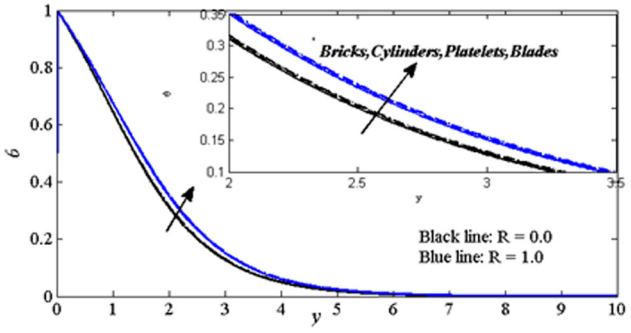

Figure 11: Impact of m on temperature θ with $R = M = 1.0$, Pr = 6.2 and $x = 0.1$.

the temperature of hybrid NF in the presence and absence of micro elements. It is noted that temperature is small in magnitude for bricks and large in magnitude for blade-shaped nanoparticles. Furthermore, the micro-rotation of the structure also enhances the temperature of hybrid NF.

Figure 12 shows the impact of micro-rotation parameter R on the skin friction of traditional NF and hybrid NF. It is noted that skin friction rises with the increase in

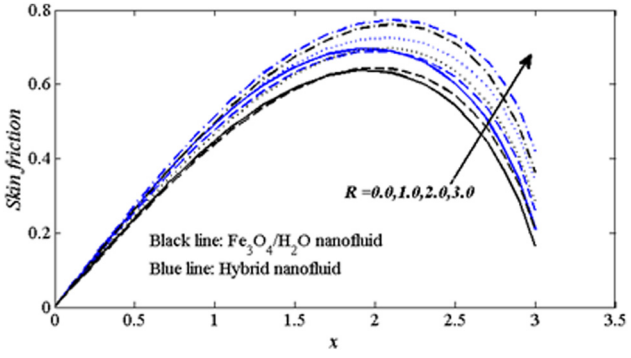

Figure 12: Impact of R on skin friction with $M = 0.5$, Pr = 6.2 and $m = 8.6$.

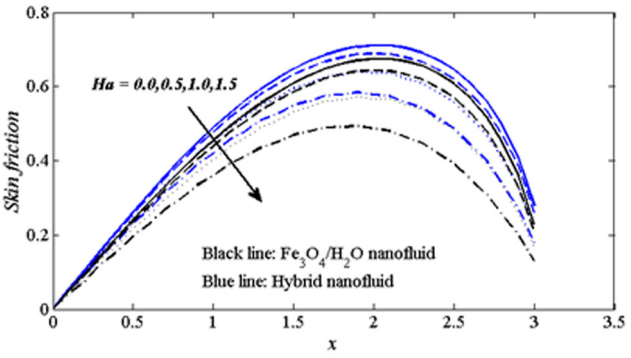

Figure 13: Impact of M on skin friction with $R = 1.0$, Pr = 6.2 and $m = 8.6$.

the micro-rotation in both types of NFs. For smaller values of micro rotation, *i.e.*, $R \leq 1$, the decrease in the skin friction is noticed for $x \leq 2$ and increases for the rest region. While on the other hand the skin friction is an increasing function of micro-rotation for $R \geq 1$ along the whole x-coordinate. The impact of magnetic parameter on the skin friction is illustrated in Figure 13 for both types of NFs. It is noted that the rise in the magnetic force reduces the skin friction along the surface of sphere in the whole cross-

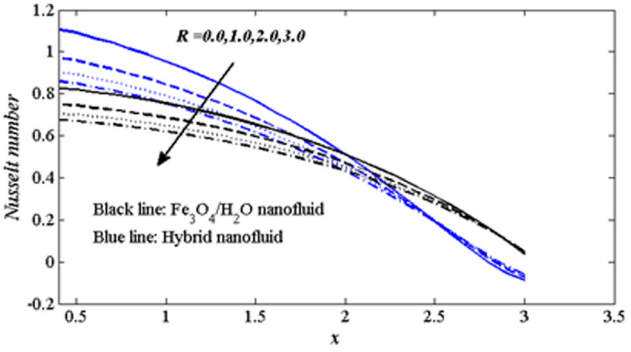

Figure 14: Impact of R on Nusselt number with $M = 0.5$, Pr = 6.2 and $m = 8.6$.

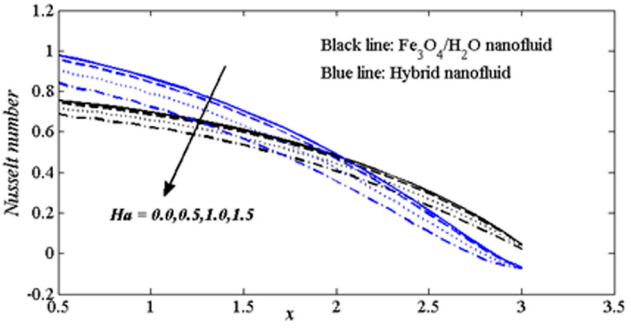

Figure 15: Impact of M on Nusselt number with $R = 1.0$, Pr = 6.2 and $m = 8.6$.

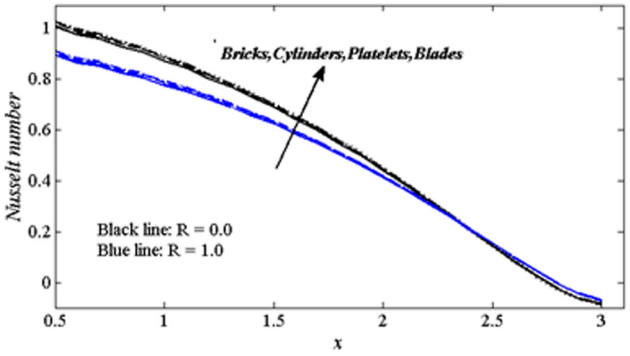

Figure 16: Impact of m on Nusselt number with R = 1.0, M = 0.5 and Pr = 6.2.

Table 4: Comparison of Nusselt number with that in the study by Lone *et al.* when Pr = 0.7, $\phi_1 = \phi_2 = 0$, Ha = 0

R	Nusselt number (present)		Nusselt number ([37])	
	$x = 0$	$x = \pi/6$	$x = 0$	$x = \pi/6$
0.0	0.4575628340	0.44790626	0.4576	0.4480
0.5	0.43348216	0.42449248	0.4337	0.4245
1.0	0.41678183	0.40787651	0.4165	0.4080
2.0	0.39365007	0.38520306	0.3930	0.3850

section. The resistance to the flow allows the decrease in the magnitude of the shear stress on the surface of the sphere. Furthermore, for hybrid NF, the magnitude of shear stress is large at the surface of the sphere as compared to Fe_3O_4/H_2O NF. The response of Nusselt number against the micro rotation is plotted in Figure 14. It is noted that the rise in micro rotation parameter R reduces the Nusselt number and the decline is Nusselt number is minimum near the origin and as away from origin this trend is reversed. The responding magnitude of Nusselt number is large in case of hybrid NF as compared to Fe_3O_4/H_2O NF. The impact of magnetic parameter Ha on the Nusselt number is depicted in Figure 15 for hybrid NF as well as traditional NF. The response of Nusselt number is also decreasing against magnetic parameter for both types of NFs under consideration. The impact of different shapes of nanoparticles on the Nusselt number is displayed in Figure 16. It is noted that the Nusselt number is small in magnitude for brick-shaped nanoparticles while large in magnitude for blade-shaped nanoparticles (Table 4).

To validate, the numerical values of Nusselt number are compared with the existing results for viscous fluid reported by Lone *et al.* [37] and it is found in good agreement.

5 Conclusions

- Both micro-rotation parameter and magnetic parameter reduces the axial velocity hybrid NF as well as traditional NF on the surface of the sphere.
- The axial velocity as well as tangential velocity is large in case of hybrid NF.
- The micro-rotation parameter rises the rotational velocity of both fluids near the surface of sphere.
- Both micro-rotation parameter and magnetic parameter rises the temperature of NFs.
- The temperature of hybrid NF is large as compared to the traditional NF.
- The skin friction is a decreasing function of magnetic field, while it is an increasing function of micro-rotation.
- Both skin friction and Nusselt number are large for hybrid nanoparticles as compared to Fe_3O_4/H_2O NF.
- The Nusselt number is a decreasing function of micro-rotation parameter and magnetic parameter.
- Both temperature and Nusselt number of hybrid NF satisfy the following order for different shapes of nanoparticles:

  bricks < cylinders < platelets < blades.

Acknowledgments: The authors acknowledge the support by Research Supporting Project Number (RSPD2024R585), King Saud University, Riyadh, Saudi Arabia.

Funding information: This work was supported by Research Supporting Project Number (RSPD2024R585), King Saud University, Riyadh, Saudi Arabia.

Author contributions: All authors have accepted responsibility for the entire content of this manuscript and approved its submission.

Conflict of interest: The authors state no conflict of interest.

References

[1] Choi SUS, Eastman JA. Enhancing thermal conductivity of fluids with nanoparticles. The Proceedings of the 1995 ASME International Mechanical Engineering Congress and Exposition. Vol. 66, San Francisco, USA, ASME, FED 231/MD; 1995. p. 99–105.

[2] Sharifi I, Shokrollahi H, Amiri S. Ferrite-based magnetic nanofluids used in hyperthermia applications. J Magnetism Magnetic Mater. 2012;324(6):903–15.

[3] de Sousa ME, van Raap MBF, Rivas PC, Zélis PM, Girardin P, Pasquevich GA, et al. Stability and relaxation mechanisms of citric

acid coated magnetite nanoparticles for magnetic hyperthermia. J Phys Chem C. 2013;117:5436–45.
[4] Walter A, Garofalo A, Parat A, Martinez H, Flesch DF, Begin-Colin S. Functionalization strategies and dendronization of iron oxide nanoparticles. Nanotechnol Rev. 2015;4:581–93.
[5] Khan WA, Waqas M, Chammam W, Asghar Z, Nisar UA, Abbas SZ. Evaluating the characteristics of magnetic dipole for shear-thinning Williamson nanofluid with thermal radiation. Comput Methods Prog Biomed. 2020;191:105396.
[6] Hosseinzadeh K, Mardani MR, Salehi S, Paikar M, Waqas M, Ganji DD. Entropy generation of three-dimensional Bödewadt flow of water and hexanol base fluid suspended by Fe_3O_4 and MoS_2 hybrid nanoparticles. Pramana. 2021;95:57.
[7] Raza A, Khan SU, Reddy YD, Goud BS, Khan MI. Dynamics of heat transport in CNTs based Darcy saturated flow: Modeling through fractional simulations. J Indian Chem Soc. 2022;99:100782.
[8] Abbasi A, Farooq W, Eldin ESM, Khan SU, Khan MI, Guedri K, et al. Heat transport exploration for hybrid nanoparticle (Cu, Fe_3O_4)-based blood flow *via* tapered complex wavy curved channel with slip features. Micromachines. 2022;13:1415.
[9] Sadiq K, Siddique I, Khan I, Khan MI, Singh A. Heat and mass transfer in a second grade nanofluids with wall slippage, heat generation and chemical reaction: Exact solutions. Int Commun Heat Mass Transf. 2023;148:107024.
[10] Waqas M, Kausar MS, Nasir M, Akram KB, Khan WA, Tamam N. Chemically reactive squeezed flow of Maxwell nanofluid confined by parallel stratified walls subjected to radiative flux. Tribol Int. 2023;189:108986.
[11] Sundar LS, Sangaraju S, Mouli KVVC. Effect of magnetic field on the thermal conductivity and viscosity of magnetic manganese oxide/ethylene glycol nanofluids: An experimental and ANFIS approach. J Magnetism Magnetic Mater. 2023;588:171386.
[12] Abbas N, Shatanawi W. Heat and mass transfer of micropolar-Casson nanofluid over vertical variable stretching riga sheet. Energies. 2022;15(14):4945.
[13] Shatnawi TA, Abbas N, Shatanawi W. Comparative study of Casson hybrid nanofluid models with induced magnetic radiative flow over a vertical permeable exponentially stretching sheet. AIMS Math. 2022;7(12):20545–64.
[14] Gumber P, Yaseen M, Rawat SK, Kumar M. Heat transfer in micropolar hybrid nanofluid flow past a vertical plate in the presence of thermal radiation and suction/injection effects. Partial Differ Equ Appl Math. 2022;5:100240.
[15] Abbas N, Rehman KU, Shatanawi W, Al-Eid AA. Theoretical study of non-Newtonian micropolar nanofluid flow over an exponentially stretching surface with free stream velocity. Adv Mech Eng. 2022;14(7):16878132221107790.
[16] El-Dawy HA, Gorla RSR. The flow of a micropolar nanofluid past a stretched and shrinking wedge surface with absorption. Case Studies in Thermal Engineering, 26, 101005.A. C. Eringen, Theory of micropolar fluids. J Math Mech. 2021;15(1):1–18.
[17] Kausar MS, Hussanan A, Waqas M, Mamat M. Boundary layer flow of micropolar nanofluid towards a permeable stretching sheet in the presence of porous medium with thermal radiation and viscous dissipation. Chin J Phys. 2022;78:435–52.
[18] Patel HR, Patel SD, Darji R. Mathematical study of unsteady micropolar fluid flow due to non-linear stretched sheet in the presence of magnetic field. Int J Thermofluids. 2022;16:100232.
[19] Thenmozhi D, Rao ME, Punithavalli R, Selvi PD. Analysis on mathematical model of convection system of micropolar fluid as Darcy-Forchheimer flow undergoes heterogeneous and homogeneous chemical reaction. Forces Mech. 2023;12:100214.
[20] Yadav PK, Yadav N. Entropy generation analysis in micropolar-couple stress fluid's flow in an inclined porous channel using Homotopy Analysis Method. Chin J Phys. 2023;16(20). doi: 10.1016/j.cjph.2023.10.024
[21] Magyari E, Chamkha AJ. Combined effect of heat generation or absorption and first-order chemical reaction on micropolar fluid flows over a uniformly stretched permeable surface: The full analytical solution. Int J Therm Sci. 2010;49(9):1821–8.
[22] Mustafa I, Shahbaz S, Ghaffari A, Muhammad T. Non-similar solution for a power-law fluid flow over a moving wedge. Alex Eng J. 2023;75:287–96.
[23] Ul Haq S, Ashraf MB. Non-similar solution of mixed convection flow of viscous fluid over curved stretching surface with viscous dissipation and entropy generation. Numerical Heat Transfer, Part B: Fundamentals. 2024;85(2):177–98.
[24] Minkowycz WJ, Sparrow EM. Local nonsimilar solutions for natural convection on a vertical cylinder. The American Society of Mechanical Engineers; 1974.
[25] Chamkha AJ, Abbasbandy S, Rashad AM, Vajravelu K. Radiation effects on mixed convection about a cone embedded in a porous medium filled with a nanofluid. Meccanica. 2013;48:275–85.
[26] Kong L, Liu G. Synchrotron-based infrared microspectroscopy under high pressure: An introduction. Matter Radi Extremes. 2021;6(6):68202. doi: 10.1063/5.0071856.
[27] Lyu X, Wang X, Qi C, Sun R. Characteristics of cavity dynamics, forces, and trajectories on vertical water entries with two spheres side-by-side. Phys Fluids. 2023;35(9):92101. doi: 10.1063/5.0166794.
[28] Qiu Y, Shi M, Guo X, Li J, Wu J, Zhou Y, et al. Sensitivity improvement in the measurement of minor components by spatial confinement in fiber-optic laser-induced breakdown spectroscopy. Spectrochim Acta Part B: At Spectrosc. 2023;209:106800. doi: 10.1016/j.sab.2023.106800.
[29] Qiu Y, Guo X, Shi M, Zhou Y, Wu J, Li J, et al. Plasma dynamics and chlorine emission characteristics on cement pastes using collinear dual-pulse laser-induced breakdown spectroscopy. Spectrochim Acta Part B: At Spectrosc. 2023;209:106799. doi: 10.1016/j.sab.2023.106799.
[30] Zhao C, Cheung CF, Xu P. High-efficiency sub-microscale uncertainty measurement method using pattern recognition. ISA Trans. 2020;101:503–14. doi: 10.1016/j.isatra.2020.01.038.
[31] Bég OA, Prasad VR, Vasu B, Reddy NB, Li Q, Bhargava R. Free convection heat and mass transfer from an isothermal sphere to a micropolar regime with Soret/Dufour effects. Int J Heat Mass Transf. 2011;54(1–3):9–18.
[32] Bisht A, Sharma R. Non-similar solution of Sisko nanofluid flow with variable thermal conductivity: a finite difference approach. Int J Numer Methods Heat Fluid Flow. 2020;31(1):345–66.
[33] Hayath TB, Ramachandran S, Vallampati RP, Bég OA. Computation of non-similar solution for magnetic pseudoplastic nanofluid flow over a circular cylinder with variable thermophysical properties and radiative flux. Int J Numer Methods Heat Fluid Flow. 2021;31(5):1475–1519.
[34] Farooq U, Hussain M, Ijaz MA, Khan WA, Farooq FB. Impact of non-similar modeling on Darcy-Forchheimer-Brinkman model for forced convection of Casson nano-fluid in non-Darcy porous media. Int Commun Heat Mass Transf. 2021;125:105312.
[35] Hussain M, Khan W, Farooq U, Razzaq R. Impact of non-similar modeling for thermal transport analysis of mixed convective flows of nanofluids over vertically permeable surface. J Nanofluids. 2023;12(4):1074–81.

[36] Waini I, Ishak A, Pop I. Radiative and magnetohydrodynamic micropolar hybrid nanofluid flow over a shrinking sheet with Joule heating and viscous dissipation effects. Neural Comput Appl. 2022;34(5):3783–94.
[37] Lone SA, Alyami MA, Saeed A, Dawar A, Kumam P, Kumam W. MHD micropolar hybrid nanofluid flow over a flat surface subject to mixed convection and thermal radiation. Sci Rep. 2022;12(1):17283.
[38] Abbasi A, Farooq W. A numerical simulation for transport of hybrid nanofluid. Arab J Sci Eng. 2020;45(11):9249–65.
[39] Khan U, Zaib A, Pop I, Bakar SA, Ishak A. Unsteady micropolar hybrid nanofluid flow past a permeable stretching/shrinking vertical plate. Alex Eng J. 2022;61(12):11337–49.
[40] Nazar R, Amin N. Free convection boundary layer on an isothermal sphere in a micropolar fluid. Int Commun Heat Mass Transf. 2002;29(3):377–86.
[41] Chu YM, Nazeer M, Khan MI, Ali W, Zafar Z, Kadry S, et al. Entropy analysis in the Rabinowitsch fluid model through inclined wavy Channel: Constant and variable properties. Int Commun Heat Mass Transf. 2020;119:104980.
[42] Khan MI, Qayyum S, Kadry S, Khan WA, Abbas SZ. Theoretical investigations of entropy optimization in electro-magneto nonlinear mixed convective second order slip flow. J Magnetics. 2020;25:8–14.
[43] Khan MI, Alzahrani F. Numerical simulation for the mixed convective flow of non-Newtonian fluid with activation energy and entropy generation. Math Methods Appl Sci. 2021;44:7766–77.
[44] Jahanshahi H, Yao Q, Khan MI, Moroz I. Unified neural output-constrained control for space manipulator using tan-type barrier Lyapunov function. Adv Space Res. 2023;71:3712–22.
[45] Li S, Ali F, Zaib A, Loganathan K, Eldin SM, Khan MI. Bioconvection effect in the Carreau nanofluid with Cattaneo–Christov heat flux using stagnation point flow in the entropy generation: Micromachines level study. Open Phys. 2023;21:20220228.
[46] Khan MI, Waqas H, Farooq U, Khan SU, Chu YM, Kadry S. Assessment of bioconvection in magnetized Sutterby nanofluid configured by a rotating disk: a numerical approach. Mod Phys Lett B. 2021;35:2150202.